

Colloidal logic-gate circuits can process environmental signals and autonomously perform tasks

Jiang-Xing Chen,^{1, a)} Jia-Qi Hu,¹ and Raymond Kapral^{2, b)}

¹⁾ Department of Physics, Hangzhou Normal University, Hangzhou 311121, China

²⁾ Chemical Physics Theory Group, Department of Chemistry, University of Toronto, Toronto, Ontario M5S 3H6, Canada

Cooperative collective dynamics is a principal determinant of the ability of synthetic micromotors to perform specific functions. However, realizing controllable and predictable collective behavior in complex physiological environments remains a significant challenge. Here, we show that collections of enzyme-coated colloids can be designed as various chemical logic gates, which subsequently can be organized into functional logic circuits. These circuits take environmental information as input signals and process it to produce output chemical species needed to achieve specific goals. The chemical computation performed by the circuit endows the active colloidal system with the ability to sense its surroundings and autonomously coordinate its collective motion. The results of simulations of several examples are presented, where self-assembled colloidal circuits can identify invasive threats by their signals, produce and deliver chemicals to the targets to suppress their activity. The results of this work can aid in the design of experimental chemical logic circuits through micromotor self-assembly that autonomously respond to environmental cues to execute specific tasks.

INTRODUCTION

Synthetic micromotors form a distinctive class of active agents that have the potential to lead to transformative applications in the physical, chemical, and biological sciences^{1–3}. In biological applications, micromotors use self-propulsion to perform a number of functions such as actively targeted drug delivery or sensing and responding to invasive bodies^{4–9}. Enzyme-powered motors feature prominently in many such applications because the chemical fuel they use is bio-compatible and bio-degradable, and experimental studies have shown how micro-colloids with Janus and random enzyme coats can be made using single enzyme species or multiple enzyme types^{10–16}.

Micromotors that sense their environments have been constructed; for example, laboratory studies have been carried out on enzyme-coated micromotors with pH-responsive nanovalves for on-demand cargo delivery¹⁷ and with DNA nanoswitches for pH sensing¹⁸; also enzymatic cascades have been shown to produce chemomechanical communication¹⁹. Such investigations prompt the development of other active and autonomous sensing paradigms. In this paper, we show how logic-gate circuits constructed from colloid-based chemical logic gates can be used to carry out computations that allow active colloidal systems to process and respond to information from their environment. The use of active colloidal chemical logic gates builds on the extensive literature dealing with the construction of chemical logic gates and logic-gate circuits in bulk phase systems^{20–34}. All standard logic gates can be built from protein enzymatic chemical reactions or from reaction kinetics that uses nucleic acid molecules. Logic-gate circuits may then be constructed through multiple coupled enzymatic logic gate reactions.

For example, various two-input gates using de novo designed proteins have been constructed³¹, and have aided in programmable design of protein circuits^{32,35}.

The general principles used to design enzymatic gates in fluid phase systems can be applied to colloidal surface enzyme coats, enabling the construction of active-colloid-based logic circuits. Several features make the construction of colloidal gates built from protein enzymatic reactions feasible. Micron-scale colloidal particles can support protein coats on their surfaces comprising an order of 10^5 molecules so that multiple surface enzymatic reactions, whose characteristics depend on the structure of the protein surface coat, can take place. Indeed, as discussed above, enzyme-coated active colloidal particles can support multiple enzymatic reactions. Models of such enzyme-coated colloids have been constructed, and simulations of their dynamics have shown that they can function as chemical logic gates³⁶. Here, we describe how systems containing colloidal particles with different logic gates can act collectively to form logic-gate circuits that can be programmed to respond to a number of different chemical inputs to produce specific chemical outputs. Through this process, we show that the colloidal system can sense the chemical composition of its environment and autonomously respond to it to carry out a given task.

Although the operation of chemical logic-gate circuits in bulk phase systems with randomly dispersed enzymes is well documented, the localized nature of the enzyme coatings on active colloidal surfaces—and the consequent reshaping of signal transmission between individual colloidal logic units—necessitates investigation to determine how these logical circuits can form through self-assembly and encode environmental input to generate collective autonomous responses. The results presented in this paper address these issues and should serve as a guide for experiment.

The outline of the paper is as follows: Section A be-

^{a)} jxchen@hdu.edu.cn

^{b)} rkapral@chem.utoronto.ca

gins with general considerations that underlie the construction of colloidal chemical logic-gate circuits. We then show how a colloidal logical circuit, with characteristics that are similar to an OR-AND-XOR circuit which was experimentally implemented in a microfluidic system²³, can be made from three linked gated colloids, and summarize the results of simulations in the truth table that provides a Boolean representation of its operation. Through several examples in Sec. B, we show how versions of this and other circuits comprising unlinked colloids can cooperatively form by self-assembly and be used to target and neutralize invasive particles that emit chemical signals detected by the circuits. Further details on the construction of the colloidal circuits and the simulation methods used to study their dynamics are given in Methods and Supporting Information.

RESULTS

A. Active colloidal logic-gate circuits

The colloidal chemical logic gates that comprise a circuit are based on reaction kinetics that takes place on enzyme-coated colloid surfaces. Simple gates can be built on colloids with a uniform coat of a single enzyme species, or inhomogeneous colloid coats with enzyme-covered and inactive domains. More complicated gates that require several enzymatic reactions for their implementation can be built on colloids with inhomogeneous coats where domains have different enzymes. Such inhomogeneous coats can also be used to add a propulsive component to the gated colloids through self-generated chemical gradients that underlie phoretic mechanisms³⁷.

In order for the logic-gate colloids to form a circuit, the chemical output of one gate must be sensed as input for the next colloid gate in the circuit, enabling signal processing. Therefore, these colloidal collectives need to coordinate and cooperate with each other. In some situations, especially for biological systems where many reactions occur in the environment, chemical species are degraded by catabolic reactions as they diffuse, so the colloids should be in sufficiently close proximity to complete the circuit. This can be achieved in various ways. Diffusiophoretic motion of colloids in the chemical gradients that are generated by the action of the gates could lead to the self-assembly of the circuit. If the colloids respond to a localized source of a chemical species, diffusiophoretic motion of all the colloids in the circuit towards the source could lead to a cluster circuit that acts where it is needed. Linker molecules could be attached to the gates that selectively lead to the formation of a bound gated cluster that acts as a circuit. The mechanism that operates to form the circuit depends on the physical context.

An OR-AND-XOR circuit

To show how a colloidal logic-gate circuit can be made

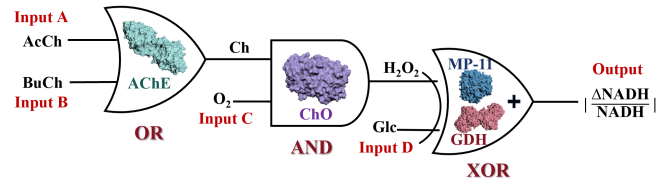
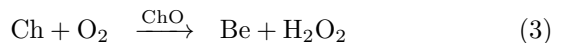


FIG. 1. Schematic depiction of the operation of the OR-AND-XOR logic circuit constructed using four enzymes, AChE, ChO, MP-11, and GDH. Details of its operation are given in the text.

from various gates, we refer to experimental work on bulk phase enzymatic systems in which an OR-AND-XOR logic-gate circuit was constructed and studied²³. The experimental logical system makes use of four enzymes: acetylcholine esterase (AChE), choline oxidase (ChO), microperoxidase-11 (MP-11), and glucose dehydrogenase (GDH) coupled to its cofactor pair NAD^+ / $NADH$. These enzymes catalyze the reactions,

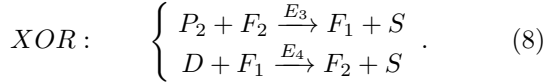
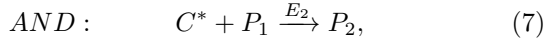
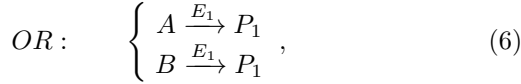


and this enzymatic reaction network underlies the logic circuit. The circuit operates as follows (see Fig. 1): The OR gate is based on Eqs. (1) and (2) where acetylcholine (input A) or butyrylcholine (input B) are hydrolyzed by AChE to form choline (Ch) that is the output of the first OR gate. (The ancillary products in these equations and elsewhere are not relevant for the operation of the circuit and their explicit dynamics need not be followed.) The AND gate based on Eq. (3) processes the Ch product (P_1) produced by the OR gate, along with O_2 (input C) taken to be in excess, to yield betaine aldehyde (Be) and H_2O_2 as products (P_2). The two biocatalysts MP-11 and GDH are used in the more complicated exclusive OR (XOR) gate described by Eqs. (4) and (5). The inputs for the XOR gate are H_2O_2 produced by the previous AND gate and glucose (Glc, input D). The operation of the circuit is read-out by following the concentration change ratio of the cofactor NADH (F_2), namely $|\Delta NADH(t)/NADH(0)|$ with $\Delta NADH(t) = NADH(t) - NADH(0)$. In the experiment, the output signal was monitored by the relative change in the absorbance of NADH and the results were used to construct the truth table for this logical circuit. Since the output is an analog signal, this circuit is made from fuzzy logic gates³⁸⁻⁴⁰. The gated action of enzymatic reactions is determined by the forms of the enzyme response curves²¹ or by filtering in experiments⁴¹. In addition, conditions on the number of enzymatic gates that can be used effectively in logic circuits have been deter-

mined⁴².

Construction of colloidal logic circuits and simulation of dynamics

The colloidal logic circuit we implement in our simulations is constructed from a simpler reaction network that focuses on the main species involved in the operation of the gates:



The input species $\{A, B, C, D\}$ and the intermediate chemical species P_1 and P_2 are processed by this network in a way that is similar to that of the inputs and the Ch and H_2O_2 species in the experimental network. The concentration of C , like O_2 in the experiment, is assumed to be constant and its value is incorporated in the reaction rate coefficient for enzyme E_2 . (Here and elsewhere, species whose concentrations are in excess are indicated by the superscript * as in C^* .) This input is assigned the Boolean value of 1. In addition, to implement the effects of open-system kinetics, we make use of a species S that undergoes reactions $S \xrightarrow{k_{cat}} A/B/D$ in the fluid phase. These reactions mimic the effects of reservoirs that supply chemical species to the system to maintain it in a nonequilibrium state, and allow the circuit to operate in the steady state regime since the input species are uniformly regenerated in the environment to compensate for their consumption in the network reactions.

For this example, we propose a colloidal circuit formed from linked colloids, and the configuration of the three colloids used in our simulations is shown in Fig. 2. To model the linker groups, the centers of mass of the colloids are connected by stiff harmonic springs to keep them in proximity so that the circuit can function effectively. Uniform coats of enzymes E_1 and E_2 are on two of the colloids. On the surface of the third colloidal sphere, one hemisphere is coated with enzyme E_3 , while the other hemisphere is coated with enzyme E_4 . The colloid complex, along with the fluid particles, reside in a simulation box with periodic boundary conditions. The system evolves by hybrid molecular dynamics-multiparticle collision dynamics⁴³⁻⁴⁶ as described in Methods and Supporting Information where full simulation details are provided.

Because the XOR gate is constructed from a colloid with a Janus coat of two different enzymes on the two hemispheres, this colloid could serve as a propulsive component for the linked cluster configuration. We could have constructed this gate from a random distribution of the two enzymes on the surface of the colloid. In fact, depending on the interaction potentials of the reactive species with the enzymes, even if all colloids had uniform

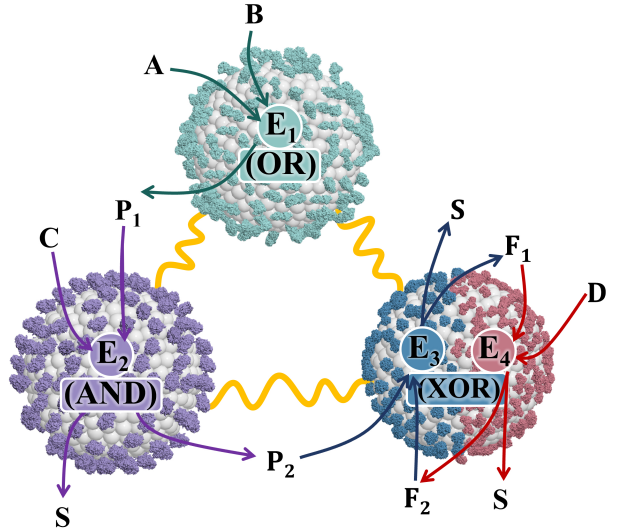


FIG. 2. The OR-AND-XOR colloidal logic-gate circuit. The circuit uses three linked colloids with coats constructed from four different enzymes as described in the text. The figure shows the reactions that underlie the OR, AND, and XOR colloidal gates. The gated colloids reside in a reactive chemical medium.

enzyme coats, active motion of the complex is possible through a mechanism similar to that of sphere dimer motors where one sphere responds to concentration gradients produced by its linked partner³⁷. Here, we have chosen the fluid-colloid interaction potentials to be the same for all species, so there is no active motion. This allows us to focus on how the circuit processes chemical signals, our primary objective in this section. In the applications presented in the next section, the potential energy interactions will not be identical for all species, and harmonic constraints will not be placed on the colloids so that they will be free to move and respond to chemical gradients to form cluster circuits.

The output of the OR-AND-XOR logic circuit to various input signals is taken to be the ratio of the concentration change of F_2 to its initial value, $\Phi(t) = |\Delta F_2(t)/F_2(0)|$. A value of $\Phi(t)$ less than 0.5 is assigned a Boolean value of “0”, while higher values are assigned “1”, so, as noted earlier, the gates we consider are fuzzy logic gates. The truth table for the circuit can be constructed from simulations of the dynamics that yield outputs for the eight possible inputs to the circuit. As examples, the temporal evolutions of the concentrations of all active species are shown in Fig. 3 for two input values to the circuit: (0110) and (1111).

Since the input C is always present and has value 1, there are eight possible inputs to the circuit specified by $(AB1D)$. Consider the input (0110) where the B species is the only other input to the circuit. Recall that for this model species F_1 and F_2 are also present in the solution. Species B activates the OR gate through the surface catalytic activity of enzyme E_1 , and this leads to the genera-

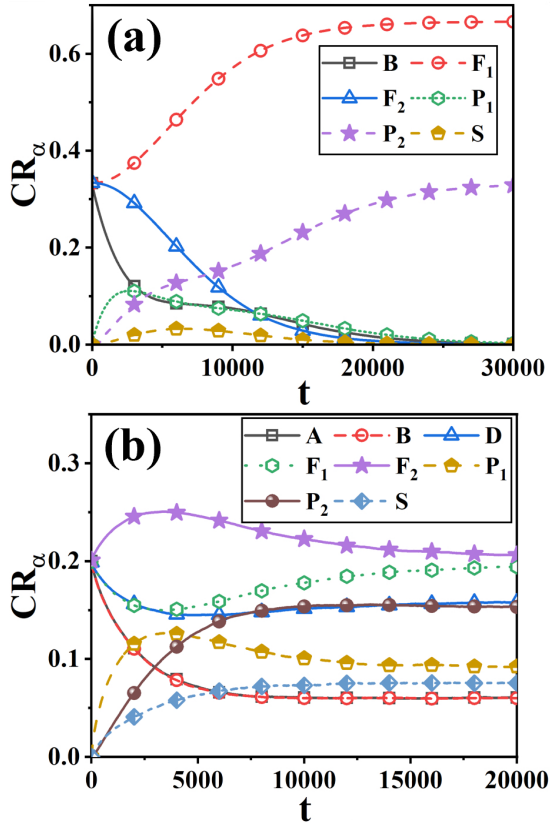


FIG. 3. Temporal evolution of species concentration ratios CR_α in the system for two (ABCD) inputs. (a) Input (0110) results in output signal “1”. (b) Input (1111) results in output signal “0”. The concentration ratio $CR_\alpha = N_\alpha(t)/N_0$, where $N_\alpha(t)$ is the number of particles of species α at time t ($\alpha = A, B, D, F_1, F_2, P_1, P_2, S$) and N_0 is the total particle number in the system.

tion of product P_1 via reactions described by Eq. (6). As observed in Fig. 3 (a), the concentration of B decreases, while that of P_1 exhibits a transient rise. The second logic gate in the circuit coated by E_2 acting as an AND gate converts P_1 to P_2 through the reaction described by Eq. (7). After reaching a maximum, the concentration of P_1 decreases, while P_2 continues to increase. Species P_2 and F_2 initiate the reaction described by Eq. (8), activating the XOR gate: enzyme E_3 on the Janus surface converts F_2 to F_1 . We note that the XOR gate can be constructed from the combination of two AND gates as shown in Fig. 4, and only the first of the two AND gates is activated with this input since species D is absent. The fluid phase reaction $S \xrightarrow{k_{cat}} B$ continuously supplies B until all F_2 is converted to F_1 . The Boolean output corresponding to input (0110) is 1.

When the input signal is (1111), species A , B and D are present, and all enzymes on the colloid surfaces are involved in the operation of the logical circuit. The evolution of the concentrations of all species is shown in Fig. 3 (b). The concentrations of A , B and D initially decrease, then gradually approach a steady state due to the bulk

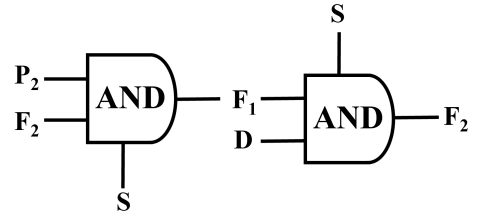


FIG. 4. The XOR gate constructed from two AND gates.

phase reaction $S \xrightarrow{k_{cat}} A/B/D$. The concentration of the intermediate product P_1 increases rapidly, since it is generated from the conversion of A and B in the OR gate reaction, and then decreases to a steady state value due to consumption at the E_2 AND gate. Species P_2 is generated and consumed in reactions (7) and (8), and its value increases to a final steady state. Species F_1 and F_2 reach a steady state that is approximately the same as the initial state, so the output of this state from $\Phi(t)$ has Boolean value 0.

The output signals from the remaining six inputs are shown in the Supporting Information. The results are summarized in Fig. 5 (a), and the corresponding truth table is presented in Fig. 5 (b). Although the dynamics underlying the OR-AND-XOR colloidal circuit differs from that in the bulk-phase experiment²³, the truth table has the same form. Therefore, colloid-based enzyme logic circuits can effectively process environmental signals.

B. Detection and suppression of invader activity

Often a goal in biomedical applications is selective targeting of an invasive body in order to terminate its activity⁴⁷. Targeting diseased cancer cells by the different biomarkers they produce is an example of such an application, and for this purpose, OR, AND and NOT protein logic gate switches have been used to distinguish cells that express different specific antigens.⁴⁸ Different types of invasive agents may give rise to distinct environmental chemical signals that are recognized by active colloidal systems, thereby forming logic circuits to respond to the threats. In this section, we provide several examples that show how colloidal logic-gate circuits can be used to perform similar tasks. In particular, we consider situations where invasive particles that are harmful to the system are present and demonstrate that self-assembled colloidal logic-gate circuits can be used to remove the threats posed by these invaders.

Single invasive species

Example 1: We suppose that the system contains a single invasive particle (termed as Invader I) that consumes chemical fuel S in its environment and produces a harmful product A,S which also signals the presence of the invader in the system. The activity of the Invader can be inhibited by a chemical P_2 that interferes

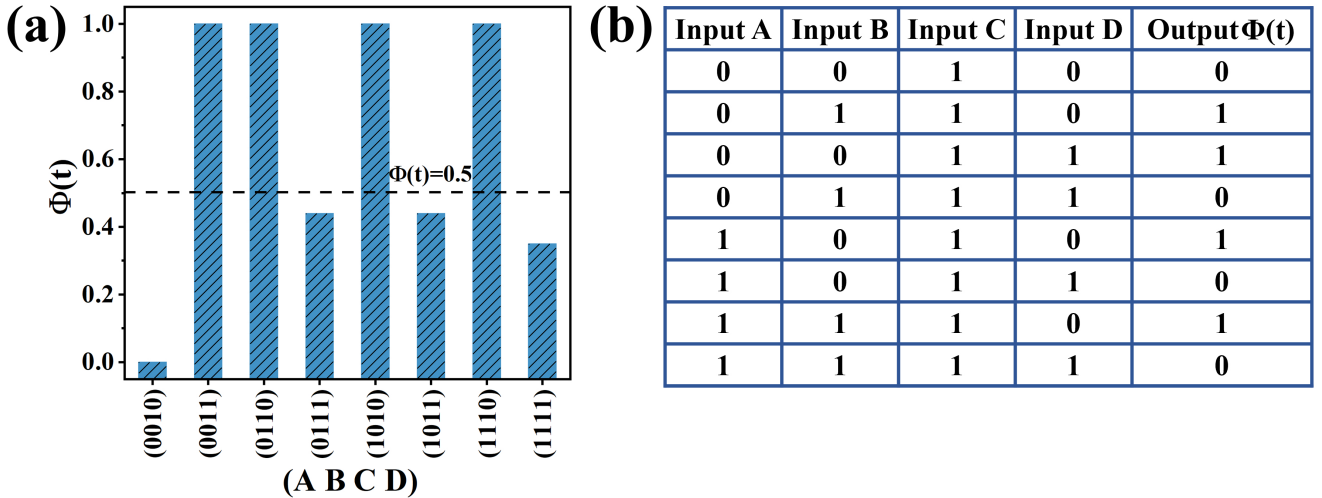


FIG. 5. (a) Bar presentation of the outputs of the OR-AND-XOR circuit. Each bar corresponds to a specific input and its corresponding output signal, $\Phi(t)$. The horizontal dashed line at $\Phi(t) = 0.5$ denotes the threshold between high and low Φ , specifying the values of the output signals as “0” and “1” respectively. (b) Truth table for the the circuit.

with the reaction that sustains it by using an inhibitor (INH) gate. Species P_2 is not present in the environment; however, the system does contain a number of (unlinked) gated colloidal particles that support different logic gates. Among these are the OR, AND and XOR gates discussed above; however, we regard the gate reactions in Eqs. (6)-(8) as generic reactions for such gates without specific reference to the experimental circuit that prompted the model equations. The Invader and the colloidal gates involved in this application are shown in Fig. 6 (a).

Initially, the system contains only three types of particles in solution: S , F_1 , and F_2 , the latter two involved in the operation of the XOR gate. Recall that the XOR gate can be constructed from two AND gates and, since species D is not present, only the AND gate involving enzyme E_3 is active. The activated circuit used in this application is shown in Fig. 7.

The colloidal system can detect the presence of the Invader by its chemical signal A, and this signal triggers a response that leads to the formation of a circuit that suppresses the activity of the Invader. From Fig. 7 one can see that the OR-AND circuit in the left box will generate the P_2 species that is needed. The evolution of the species concentrations are as follows (Fig. 6 (b)): The initial increase in the concentration of A and a concomitant decrease in S due to the presence of the Invader produces a concentration gradient of A around I . Once the OR colloid senses the A gradient, it experiences positive chemotactic motion toward I , since A is a substrate for E_1 . In the simulation, this directed migration is realized by a diffusiophoretic mechanism involving specific energy parameters (see Supporting Information). The activated logic circuit generates P_1 on the OR gate. Likewise, the AND colloid senses the gradient field of P_1 around the OR colloid and moves closer toward it, and they approach I together. Fig. 6 (c) shows the decrease

in the separation between I and the AND colloid. The organization of the OR-AND part of the circuit occurs through substrate-driven chemotaxis^{49,50}. In such cascade chemotaxis each enzyme independently follows its own substrate gradient, which in turn is produced by the preceding enzymatic reaction in the circuit⁵¹. As shown in Fig. 6 (d), this process results in an increase in the local concentration c_{P_2} of P_2 in the vicinity of I , and when the concentration of P_2 exceeds a critical threshold P_{2c} , the activity of I is suppressed by the INH gate. If the value P_{2c} required for suppression I is increased, the AND colloid must move closer to I , resulting in a smaller separation, as seen in Fig. 6 (c). Similarly, the active lifetime t_x , from the entry of I into the system until its chemical activity is suppressed, also increases, as shown in Fig. 6 (e).

Although the task of suppressing the activity of the invader has been accomplished, the system is still left with an unused concentration of P_2 , an unwanted possibly harmful agent such as H_2O_2 . The second AND colloidal gate in the right box in Fig. 7 is then used to remove this species. The continuous production of S through this pathway effectively replenishes the originally-present S molecules in the bulk solution. In addition, this newly generated S establishes a feedback loop: it diffuses towards the Invader and serves as the precursor for the sustained generation of A, thereby maintaining the stable A and P_1 concentration gradients that are essential for OR (E_1) and AND (E_2) sensing, respectively.

Example 2: In the previous example, the logical circuit was assembled in response to an input of A (input signal (1010); recall C takes Boolean value 1). Other inputs to a system containing colloids with he same gates can elicit different responses. For example, suppose that the fluid phase has nonzero initial concentrations of S, F_1 and F_2 species, with $c_{F_1} = c_{F_2}$. At $t = 0$ an invasive

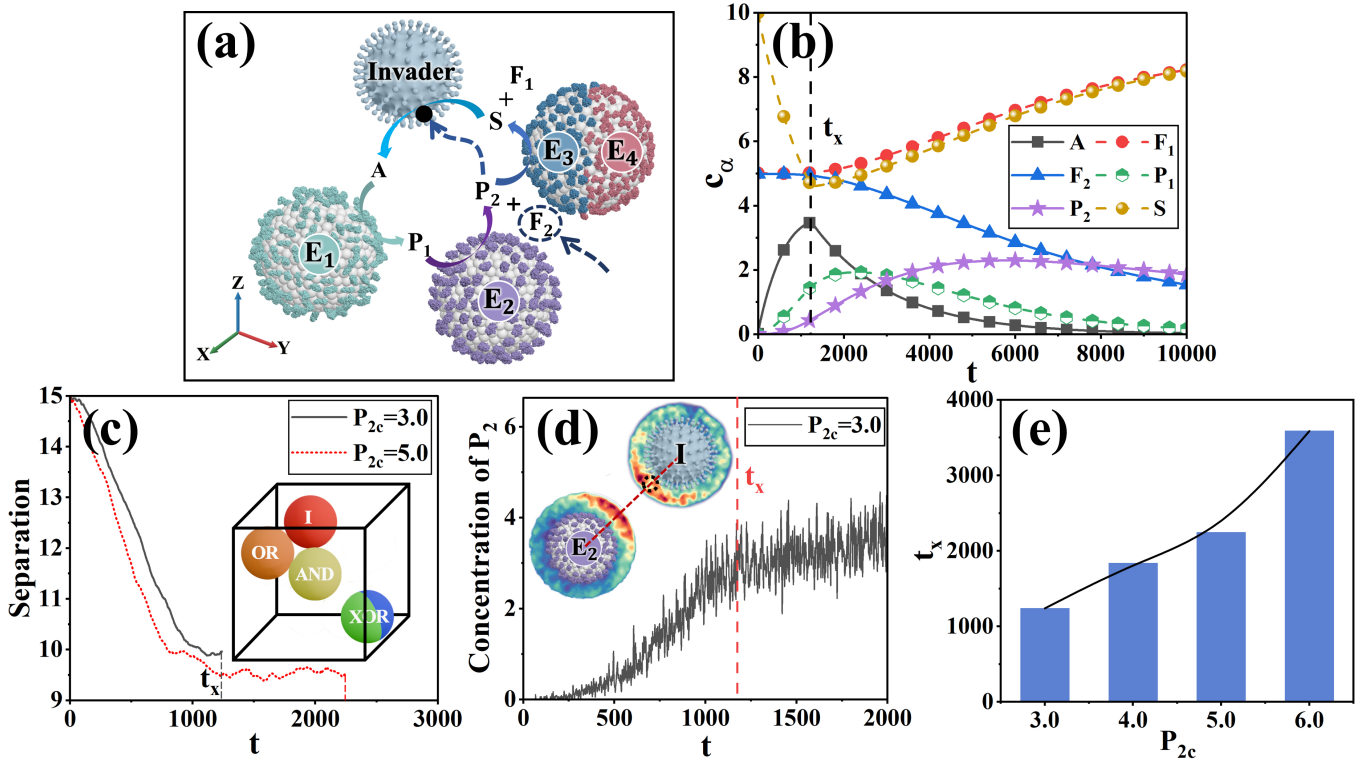


FIG. 6. (a) Schematic diagram shows the kinetics of the enzymatic logic-gate circuit responding to an Invader. The $S \rightarrow A$ chemical activity of I can be inhibited by a species P_2 when its concentration exceeds a critical value, as indicated by the small solid black circle in the diagram. (b) Temporal evolution of the six species concentrations c_α in the system. The vertical dashed line marks the lifetime t_x of I when its activity is terminated. (c) The evolution of the separation between the AND colloid (E_2) and I at different critical concentrations P_{2c} . The inset shows the positions of all colloids in the system at the moment I loses activity. (d) The temporal evolution of the concentration c_{P_2} of P_2 around I (plotted from the dashed circular area near I in the inset). The inset shows the concentration field of P_2 around I ($4.0 < r < 7.0$), and of A around E_2 ($4.0 < r < 7.0$). The symbol P_{2c} denotes the critical concentration of P_2 that causes I to lose its activity. (e) The lifetime t_x for several values of the critical concentration P_{2c} .

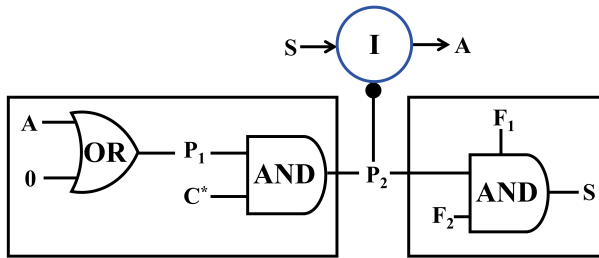


FIG. 7. The OR-AND-AND-INH circuit used in this model.

species that consumes S and produces a signal chemical D is introduced into the system. The activity of the invader will be suppressed if the concentration ratio F_2/F_1 is sufficiently high. The gated colloidal system will respond in a simple way to such a threat. The input signal for species D (0011) will activate the right AND gate in the composite XOR gate shown in Fig. 4, with other gates remaining inactive. The system is shown in Fig. 8 (a). As time evolves, the concentration of F_2 increases (Fig. 8 (b)), thereby increasing the F_2/F_1 ratio.

Concentration gradients of D are established around I and the XOR Janus colloid. These gradients cause the XOR colloid to move closer to I through substrate-driven chemotaxis. Fig. 8 (c) shows how the separation between the Janus XOR colloid and I decreases. The gate reaction on E_4 results in a higher concentration of F_2 surrounding I (Fig. 8 (a)). When the F_2/F_1 ratio exceeds the critical concentration $c_{F_{2c}}$, the catalytic activity of I is inhibited by an INH gate as in the previous example. The inset on the lower right in Fig. 8 (c) shows an instantaneous configuration of all colloidal particles, where the close proximity of the Janus colloid to the I particle can be seen. The upper middle inset of this figure shows how t_x increases with increasing F_{2c} concentration.

In the Supporting Information we give other examples, including cases where the invasive body produces more than a single signal chemical species.

Two invasive species

In some circumstances, the system may be exposed to more than a single type of invasive species. In this section, we show that ensembles of enzyme-coated colloidal motors can be configured to implement distinct logic circuits that collectively respond to and suppress multiple invaders. In particular, we consider situations where two different invasive species are introduced into the system: Invader 1 (I_1) and Invader 2 (I_2) can convert S-particle fuel in the environment to signal A and B particles, respectively. An enzyme-based logic circuit suppresses the activity of both invader species. The reactive fluid system contains a single colloid functionalized with enzyme 2 (\bar{E}_2) that acts as an AND gate and eight colloids functionalized with enzyme 1 (\bar{E}_1) that act as OR gates, together with invader species. The overlines on enzymes are introduced to stress that enzymes used to build AND and OR gates are not the same as those

for the single invader examples.

The colloidal reaction network is shown in Fig. 9 (a) and the corresponding simplified logic circuit is presented in Fig. 9 (b): when particle A encounters the AND gate with \bar{E}_2 , it is converted to P_1 in the presence of species C; subsequently P_1 is transformed into P_2 on the OR gates with \bar{E}_1 . The OR gate colloids can also convert particle B into P_2 . The product P_2 then inhibits the activity of the invaders through the action of an INH gate. Particles A and B are degraded to S in the environment by catabolic reactions $A/B \xrightarrow{k_{cat}} S$ on long timescales.

The colloidal circuit is completed by self-assembly through substrate-driven chemotaxis, similar to that for a single invasive species: the AND gate co-migrates with the downstream OR-gate colloids toward I_1 , resulting in a rapid increase in the local concentration c_{P_2} of P_2 around I_1 (solid lines in Fig. 9 (c)). Since B also functions as the direct substrate for the OR-gate colloids, they also move by chemotaxis toward I_2 , thus increasing P_2 concentration in the vicinity of I_2 (dashed lines in Fig. 9 (c)). Consequently, the OR-gate colloids can accumulate either around I_1 or I_2 depending on local environmental conditions.

Compared to the increase of P_2 around I_1 induced by AND (\bar{E}_2) – OR (\bar{E}_1) cascade chemotaxis, the direct chemotactic response of OR-gate colloids to their other substrate B leads to a more rapid accumulation of P_2 around I_2 . This is evident in the c_{P_2} curves in Fig. 9 (c) where the concentration of P_2 is higher around I_2 than I_1 . When identical critical thresholds P_{2c} are applied to both I_1 and I_2 , for the given simulation parameters, I_2 is inhibited earlier than I_1 ($t_{x2} < t_{x1}$). When the chemical activity of I_2 is suppressed at $t = t_{x2}$, the production of B stops, leading to a rapid decrease in P_2 concentration around I_2 (dashed-line curve in Fig. 9 (c)). The P_2 concentration around I_1 shows the opposite trend (cf. concentrations at $t = t_{x2}$ and t_{x1} (lower) in the insets). The OR-colloid probability density shown in Fig. 9 (d) is bimodal, indicating accumulation of OR colloids near both I_1 and I_2 . Consequently, the OR colloids in the logic circuit self-organize as a result of changes due the invasive species. Moreover, Fig. 9 (e) shows that increasing the value of P_{2c} prolongs the lifetimes of both I_1 and I_2 , while the lifetime gap, $t_{x1}-t_{x2}$, also widens.

DISCUSSION

The research reported in this paper showed how logical circuits constructed from colloid-based chemical logic gates can be used to sense chemical signals and respond to those signals by performing specified functions. Chemical logic gates can be built using enzyme or nucleic acid reaction kinetics, as demonstrated in previous experimental investigations of bulk-phase and micro-fluidic systems. Enzymatic reactions are especially convenient for this purpose because active colloids with various enzyme coats have been made and their properties have

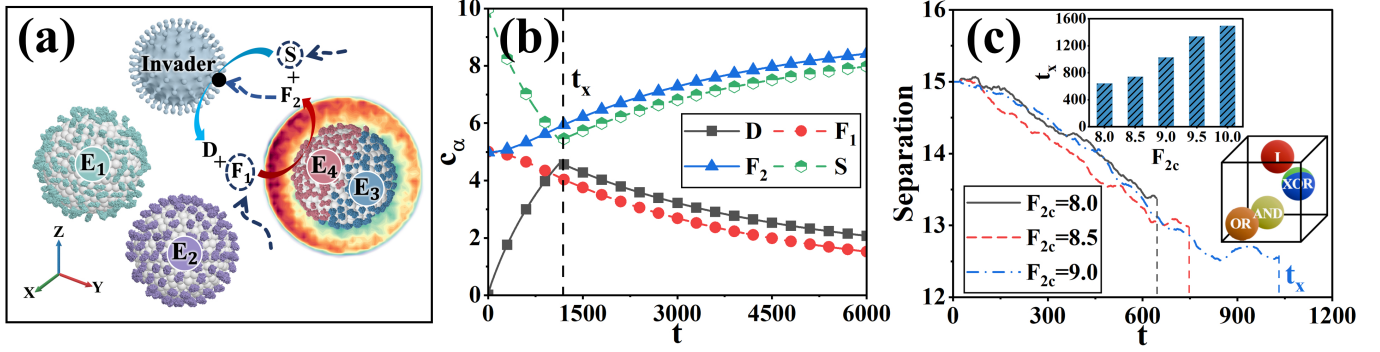


FIG. 8. (a) Picture of the logical circuit activating a portion of the XOR colloid in response to an invasive species that emits species D . The $S \rightarrow D$ activity of I is inhibited by the action of an INH gate for a high ratio of F_2/F_1 concentrations in the domain ($4.0 < r < 7.0$) around the Invader. The asymmetric concentration profile of D around the XOR Janus colloid is also shown in the figure. (b) Time-dependent evolution of four species concentrations in the system. (c) The evolution of the separation between the Janus colloid and I at different critical concentrations F_{2c} . The upper middle inset shows the lifetime t_x as a function of F_{2c} , while the lower right inset shows the colloidal configuration.

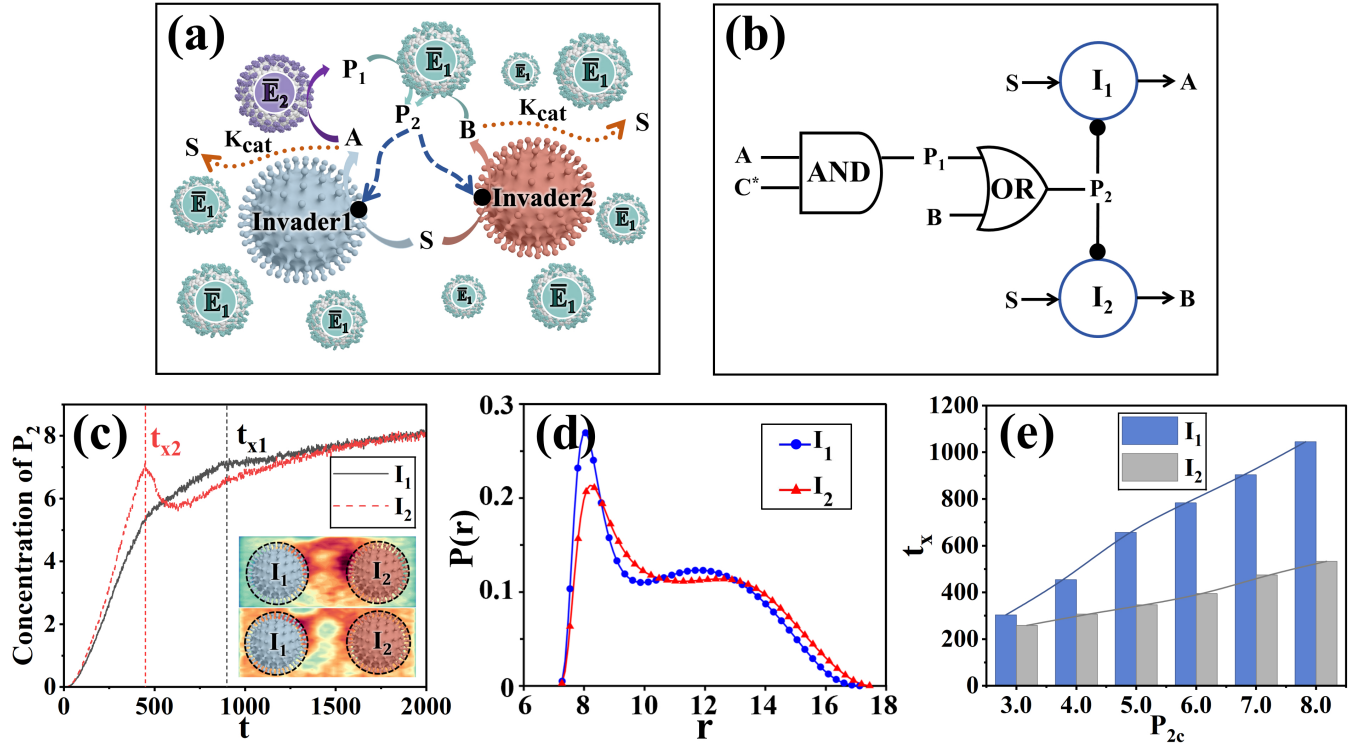


FIG. 9. (a) Diagram shows the kinetics of the enzymatic logic-gate circuit responding to two different Invaders, I_1 and I_2 . The simulation system contains one AND colloid coated by \bar{E}_2 and eight OR colloids coated by \bar{E}_1 . (b) The AND-OR-INH circuit used in this model. (c) The temporal evolution of the concentration c_{P_2} around I_1 (solid lines) and I_2 (dashed lines). These concentrations are averages over spherical shells ($4.0 < r < 4.5$) surrounding I_1 and I_2 , respectively. The insets show the concentration profiles of P_2 around I_1 and I_2 at $t=t_{x2}$ (upper) and $t=t_{x1}$ (lower), respectively. (d) The radial probability distribution $P(r)$ of OR-gates around I_1 and I_2 at $t=500$. The results are determined from 20 realizations of the dynamics. (e) The dependence of the lifetimes t_{x1} and t_{x2} on the critical concentration $c_{P_{2c}}$.

been studied.

Colloidal logic circuits are built by coupling chemical reactions on different gated colloids to form a chemical network that can process chemical signals. In order for the circuit to form and function, the colloids that com-

prise the circuit should be in close proximity, so the output of one gate could serve as input to another gate. This can be achieved by design through specific linking molecules, substrate-driven diffusiophoretic motion or active self-propulsion. The operation of the fuzzy logical

circuits formed in this way can be classified in terms of the Boolean operations they perform, so that the output of the circuit is the result of a chemical computation.

The dynamical simulations have served to highlight two aspects that determine how colloidal chemical logic-gate circuits operate: processing chemical signals, and circuit assembly and dynamics related to function. Once a circuit is specified by its constituent gates and their connections, its output for given inputs is encoded in the truth table (cf. Sec. A). For circuits made of colloidal gates, this requires the selection of coated colloids that catalyze specific chemical reactions that underlie the different gate functions. The gate reactions in the circuits then form a chemical network that processes input chemical signals to yield the desired output species. The logic gate structure that underlies the chemical network and the Boolean representation of the chemical inputs and outputs provides a way to construct the chemical networks needed in applications⁵². Thus, the representation of the chemical network in terms of logical circuits comprising chemical logic gates provides an organizing structure for the often-complex chemical kinetics that these active systems possess.

Considering general scenarios that utilize colloidal logic gates, instead of initially linking the colloids to form a circuit, the system should be able to respond to input by autonomously self-assembling the colloids needed to build the circuit. For this purpose, one must make use of the intermediate chemicals involved in the circuit and its active properties, rather than only its final chemical output. Substrate-driven chemotaxis can play an important role in such self-assembly, but so can colloid self-propulsion and dynamical linking. Once the circuit is constructed and operational, the chemical output must be put to use. This could involve movement of the colloidal circuit to the vicinity of some target, as was the case for the destruction of invasive species discussed in Sec. B. Although we described how self-propulsion of gated colloids can be included in the dynamical description of colloidal circuits, our examples did not make use of this effect. Other applications, such as targeted pick-up and delivery of cargo, could use different strategies involving the self-propulsion of the colloids comprising the circuit.

It should be possible to construct chemical logic-gate systems whose response is not limited to a specific application. For instance, consider a system of many active gated colloidal particles supporting a number of different logical gates. Such a system can process many different input signals and, when presented with a specific chemical signal, it will respond by assembling a prescribed subset of gated colloids to yield a corresponding output. The nature of the collective dynamics of such large ensembles of gated colloids and their responses to input chemical signals merit further study.

METHODS

This Methods section provides a qualitative summary of relevant aspects of the simulation methods used to obtain the results in the main text. It also serves as a guide to the complete description of all simulation details that are given in the Supporting Information (SI).

Colloid model A spherical colloid is constructed from point particles that are randomly distributed inside a sphere with radius R , along with coarse-grained enzyme beads that are uniformly distributed on the spherical surfaces of the colloid. If the colloid has an enzyme coat comprising two more enzymes or inactive surface beads, non-uniform distributions that depend on the physical context are implemented. The point particles and the enzyme beads are connected by harmonic springs. Invader species are modeled by single spheres with radius R_I .

Enzyme logic gate models Enzyme-catalyzed reactions on the surface of a colloid are carried out using a particle-based model. When a solution substrate reactive particle enters the reaction zone of an enzyme bead, a product particle is formed with a specified probability. The reactive dynamics conserves mass, momentum and energy. The reaction rule depends on the identity of the logic gate; for instance, an AND gate has two inputs, and the reaction rule is constructed so that the product is produced only when two substrates are in the reaction zone. In addition, since the reactions are gated, restrictions are placed on the local concentrations of substrate species to enforce gate conditions.

System dynamics The dynamics of the entire system is described by hybrid Molecular Dynamics-Multi-Particle Collision (MD-MPC) dynamics⁴³⁻⁴⁶. In MPC dynamics interactions among the fluid particles are taken into account through multiparticle collisions in cells with linear dimension a_0 . In the MD steps the system evolves by Newton's equations of motion with forces determined from potential functions. Enzymatic catalytic reactions occur at each MD step. Fluid phase reactions are described by reactive multiparticle collision dynamics⁵³. The simulation volume is a three-dimensional box with volume $V = L_x \times L_y \times L_z$, which contains the colloids along with a large number $N_S \sim 10^6$ of explicit solution molecules.

Interaction potentials The interaction potential between solvent particles and colloid surface enzyme beads is either a repulsive Lennard-Jones (LJ) potential, or a truncated attractive LJ potential, depending on the application. The colloids interact with each other through repulsive LJ potentials, unless linked colloid configurations are used. These interactions are characterized by energy ϵ and distance σ parameters.

Dimensionless units All quantities in the text are reported in dimensionless units based on energy ϵ , mass m_s , and distance a_0 , parameters: $t(m_s a_0^2 / \epsilon)^{1/2} \rightarrow t$, $r/a_0 \rightarrow r$, and $k_B T/\epsilon \rightarrow T$.

¹G. Gompper, R. G. Winkler, T. Speck, A. Solon, C. Nardini, F. Peruani, H. Löwen, R. Golestanian, U. B. Kaupp, L. Alvarez, T. Kiørboe, E. Lauga, W. C. K. Poon, A. DeSimone, S. Muiños-Landin, A. Fischer, N. A. Söker, F. Cichos, R. Kapral, P. Gaspard, M. Ripol, F. Sagués, A. Doostmohammadi, J. M. Yeomans, I. S. Aranson, C. Bechinger, H. Stark, C. K. Hemelrijck, F. J. Nedelec, T. Sarkar, A. T. Aryaksama, M. Lacroix, G. Duclos, V. Yashunsky, P. Silberzan, M. Arroyo, and S. Kale, “The 2020 motile active matter roadmap,” *J. Phys.: Condens. Matter* **32**, 193001 (2020).

²J. Wang, *Nanomachines: Fundamentals and Applications* (Wiley-VCH, 2013).

³X. Ju, C. Chen, C. M. Oral, S. Sevim, R. Golestanian, M. Sun, N. Bouzari, X. Lin, M. Urso, J. S. Nam, Y. Cho, X. Peng, F. C. Landers, S. Yang, A. Adibi, N. Taz, R. Wittkowski, D. Ahmed, W. Wang, V. Magdanz, M. Medina-Sánchez, M. Guix, N. Bari, B. Behkam, R. Kapral, Y. Huang, J. Tang, B. Wang, K. Morozov, A. Leshansky, S. A. Abbasi, H. Choi, S. Ghosh, B. Borges Fernandes, G. Battaglia, P. Fischer, A. Ghosh, B. Jurado Sánchez, A. Escarpa, Q. Martinet, J. Palacci, E. Lauga, J. Moran, M. A. Ramos-Docampo, B. Städler, R. S. Herrera Restrepo, G. Yossifon, J. D. Nicholas, J. Ignés-Mullol, J. Puigmartí-Luis, Y. Liu, L. D. Zarzar, C. W. I. Shields, L. Li, S. Li, X. Ma, D. H. Gracias, O. Velev, S. Sánchez, M. J. Esplandiu, J. Simmchen, A. Lobosco, S. Misra, Z. Wu, J. Li, A. Kuhn, A. Nourhani, T. Maric, Z. Xiong, A. Aghakhani, Y. Mei, Y. Tu, F. Peng, E. Diller, M. S. Sakar, A. Sen, J. Law, Y. Sun, A. Pena-Francesch, K. Villa, H. Li, D. E. Fan, K. Liang, T. J. Huang, X.-Z. Chen, S. Tang, X. Zhang, J. Cui, H. Wang, W. Gao, V. Kumar Bandari, O. G. Schmidt, X. Wu, J. Guan, M. Sitti, B. J. Nelson, S. Pané, L. Zhang, H. Shahsavan, Q. He, I.-D. Kim, J. Wang, and M. Pumera, “Technology roadmap of micro/nanorobots,” *ACS Nano* **19**, 24174–24334 (2025).

⁴J. Lin, C. Lian, L. Xu, Z. Li, Q. Guan, W. Wei, H. Dai, and J. Guan, “Hyperglycemia targeting nanomotors for accelerated healing of diabetic wounds by efficient microenvironment remodeling,” *Adv. Funct. Mater.* **35**, 2417146 (2025).

⁵A. C. Hortelão, C. Simó, M. Guix, S. Guallar-Garrido, E. Julián, D. Vilela, L. Rejc, P. Ramos-Cabrer, U. Cossío, V. Gómez-Vallejo, T. Patiño, J. Llop, and S. Sánchez, “Swarming behavior and in vivo monitoring of enzymatic nanomotors within the bladder,” *Sci. Robot.* **6**, eabd2823 (2021).

⁶J. Wang, B. J. Toebe, A. S. Plachokova, Q. Liu, D. Deng, J. A. Jansen, F. Yang, and D. A. Wilson, “Self-propelled pIga micromotor with chemotactic response to inflammation,” *Adv. Healthc. Mater.* **9**, 1901710 (2020).

⁷S. Tang, F. Zhang, H. Gong, F. Wei, J. Zhuang, E. Karshalev, B. Esteban-Fernández de Ávila, C. Huang, Z. Zhou, Z. Li, *et al.*, “Enzyme-powered janus platelet cell robots for active and targeted drug delivery,” *Sci. Robot.* **5**, eaba6137 (2020).

⁸J. Li, B. Esteban-Fernández de Ávila, W. Gao, L. Zhang, and J. Wang, “Micro/nanorobots for biomedicine: Delivery, surgery, sensing, and detoxification,” *Sci. Robot.* **2**, eaam6431 (2017).

⁹L. Reinisová, S. Hermanová, and M. Pumera, “Micro/nanomachines: what is needed for them to become a real force in cancer therapy?” *Nanoscale* **11**, 6519–6532 (2019).

¹⁰S. Sattayasamitsathit, K. Kaufmann, M. Galarnyk, R. Vazquez-Duhalt, and J. Wang, “Dual-enzyme natural motors incorporating decontamination and propulsion capabilities,” *RSC Adv.* **4**, 27565–27570 (2014).

¹¹P. Schattling, B. Thimgholm, and B. Städler, “Enhanced diffusion of glucose-fueled janus particles,” *Chem. Mater.* **27**, 7412–7418 (2015).

¹²M. Fernández-Medina, M. A. Ramos-Docampo, O. Hovorka, V. Salgueirín, and B. Städler, “Recent advances in nano- and micromotors,” *Adv. Funct. Mater.* **30**, 1908283 (2020).

¹³P. S. Schattling, M. A. Ramos-Docampo, V. Salgueirín, and B. Städler, “Double-fueled janus swimmers with magnetotactic behavior,” *ACS Nano* **11**, 3973 (2017).

¹⁴X. Ma, A. Jannasch, U.-R. Albrecht, K. Hahn, A. Miguel-López, E. Schäffer, and S. Sánchez, “Enzyme-powered hollow mesoporous janus nanomotors,” *Nano Lett.* **15**, 7043–7050 (2015).

¹⁵T. Patiño, N. Feiner-Gracia, X. Arqué, A. Miguel-López, A. Jannasch, T. Stumpp, E. Schäffer, L. Albertazzi, and S. Sánchez, “Influence of enzyme quantity and distribution on the self-propulsion of non-janus urease-powered micromotors,” *J. Am. Chem. Soc.* **140**, 7896–7903 (2018).

¹⁶X. Liu, Y. Wang, Y. Peng, J. Shi, W. Chen, W. Wang, and X. Ma, “Urease-powered micromotors with spatially selective distribution of enzymes for capturing and sensing exosomes,” *ACS Nano* **17**, 24343 (2023).

¹⁷A. Llopis-Lorente, A. Garcia-Fernandez, N. Murillo-Cremaes, A. C. Hortelão, T. Patino, R. Villalonga, F. Sancenon, R. Martinez-Manez, and S. Sánchez, “Enzyme-powered gated mesoporous silica nanomotors for on-command intracellular payload delivery,” *ACS Nano* **13**, 12171–12183 (2019).

¹⁸T. Patino, A. Porchetta, A. Jannasch, A. Lladó, T. Stumpp, E. Schäffer, F. Ricci, and S. Sánchez, “Self-sensing enzyme-powered micromotors equipped with ph-responsive dna nanoswitches,” *Nano Lett.* **19**, 3440–3447 (2019).

¹⁹Y.-C. Tseng, J. Song, J. Zhang, E. Shandilya, and A. Sen, “Chemomechanical communication between liposomes based on enzyme cascades,” *J. Am. Chem. Soc.* **146**, 16097–16104 (2024).

²⁰M. Sugita and N. Fukuda, “Functional analysis of chemical systems in vivo using a logical circuit equivalent: Iii. analysis using a digital circuit combined with an analogue computer,” *J. Theor. Biol.* **5**, 412–425 (1963).

²¹A. Arkin and J. Ross, “Computational functions in biochemical reaction networks,” *Biophys. J.* **67**, 560–578 (1994).

²²G. Seelig, D. Soloveichik, D. Y. Zhang, and E. Winfree, “Enzyme-free nucleic acid logic circuits,” *Science* **314**, 1585–1588 (2006).

²³T. Niazov, R. Baron, E. Katz, O. Lioubashevski, and I. Willner, “Concatenated logic gates using four coupled biocatalysts operating in series,” *Proc. Natl. Acad. Sci. U.S.A.* **103**, 17160–17163 (2006).

²⁴R. Unger and J. Moult, “Towards computing with proteins,” *Proteins* **63**, 53–64 (2006).

²⁵E. Katz and V. Privman, “Enzyme-based logic systems for information processing,” *Chem. Soc. Rev.* **39**, 1835 (2010).

²⁶T. Miyamoto, S. Razavi, R. DeRose, and T. Inoue, “Synthesizing biomolecule-based boolean logic gates,” *ACS Synth. Biol.* **2**, 72–82 (2013).

²⁷Y.-J. Chen, N. Dalchau, N. Srinivas, A. Phillips, L. Cardelli, D. Soloveichik, and G. Seelig, “Programmable chemical controllers made from dna,” *Nat. Nanotechnol.* **8**, 755–762 (2013).

²⁸E. Katz, “Enzyme-based logic gates and networks with output signals analyzed by various methods,” *ChemPhysChem* **18**, 1688–1713 (2017).

²⁹E. Katz, A. Poghossian, and M. J. Schöning, “Enzyme-based logic gates and circuits—analytical applications and interfacing with electronics,” *Analytical and Bioanalytical Chemistry* **409**, 81–94 (2017).

³⁰X. J. Gao, L. S. Chong, M. S. Kim, and M. B. Elowitz, “Programmable protein circuits in living cells,” *Science* **361**, 1252–1258 (2018).

³¹Z. Chen, R. D. Kibler, A. Hunt, F. Busch, J. Pearl, M. Jia, Z. L. VanAernum, B. I. M. Wicky, G. Dods, H. Liao, M. S. Wilken, C. Ciarlo, S. Green, H. El-Samad, J. Stamatoyannopoulos, V. H. Wysocki, M. C. Jewett, S. E. Boyken, and D. Baker, “De novo design of protein logic gates,” *Science* **368**, 78–84 (2020).

³²Z. Chen and M. B. Elowitz, “Programmable protein circuit design,” *Cell* **184**, 2284–2301 (2021).

³³D. S. Winston and D. D. Boehr, “Catalyst-based biomolecular logic gates,” *Catalysts* **12**, 712 (2022).

³⁴J. Xu, *Biological Computing* (Springer, 2025).

³⁵Z. Chen, “Protein circuit design using de novo proteins,” *Trends Biotechnol.* **41**, 593–594 (2023).

³⁶J.-X. Chen, J.-Q. Hu, and R. Kapral, “Chemical logic gates on active colloids,” *Adv. Sci.* **11**, 2305695 (2024).

³⁷G. Rückner and R. Kapral, “Chemically powered nanodimers,”

Phys. Rev. Lett. **98**, 150603 (2007).

³⁸R. M. Zadegan, M. D. E. Jepsen, L. L. Hildebrandt, V. Birkedal, and J. Kjems, “Construction of a fuzzy and boolean logic gates based on dna,” Small **11**, 1811–1817 (2015).

³⁹P. L. Gentili, “The fuzziness of the molecular world and its perspectives,” Molecules **23**, 2074 (2018).

⁴⁰J. Andréasson and U. Pischel, “Molecules with a sense of logic: a progress report,” Chem. Soc. Rev. **44**, 1053–1069 (2015).

⁴¹O. Zavalov, V. Bocharova, V. Privman, and E. Katz, “Enzyme-based logic: Or gate with double-sigmoid filter response,” J. Phys. Chem. B **116**, 9683–9689 (2012).

⁴²V. Privman, G. Strack, D. Solenov, M. Pita, and E. Katz, “Optimization of enzymatic biochemical logic for noise reduction and scalability: how many biocomputing gates can be interconnected in a circuit?” J. Phys. Chem. B **112**, 11777–11784 (2008).

⁴³A. Malevanets and R. Kapral, “Mesoscopic model for solvent dynamics,” J. Chem. Phys. **110**, 8605–8613 (1999).

⁴⁴A. Malevanets and R. Kapral, “Solute molecular dynamics in a mesoscale solvent,” J. Chem. Phys. **112**, 7260–7269 (2000).

⁴⁵R. Kapral, “Multiparticle collision dynamics: Simulation of complex systems on mesoscales,” in *Advances in Chemical Physics*, Vol. 140 (John Wiley & Sons, 2008) pp. 89–146.

⁴⁶G. Gompper, T. Ihle, D. M. Kroll, and R. G. Winkler, “Multiparticle collision dynamics: A particle-based mesoscale simulation approach to the hydrodynamics of complex fluids,” in *Advanced Computer Simulation Approaches for Soft Matter Sciences III* (Springer, 2009) pp. 1–87.

⁴⁷Y. Han, Y. Ma, M. Pei, S. Yin, J. Wang, L. Guo, Y. Fang, W. Guo, C. Deng, S. Zhao, X. Lu, J. J. Xi, H. Zhang, and P. R. Chen, “Intratumoural vaccination via checkpoint degradation-coupled antigen presentation,” Nature (2026).

⁴⁸M. J. Lajoie, S. E. Boyken, A. I. Salter, J. Bruffey, A. Rajan, R. A. Langan, A. Olshefsky, V. Muhunthan, M. J. Bick, M. Gewe, *et al.*, “Designed protein logic to target cells with precise combinations of surface antigens,” Science **369**, 1637–1643 (2020).

⁴⁹A. Sapre, X. Lu, Y.-C. Tseng, M. Mansour, N. S. Mandal, and A. Sen, “Non-reciprocal chemotactic movement in enzyme cascade under flow-free conditions,” Cell Rep. Phys. Sci. **6**, 102666 (2025).

⁵⁰A. Somasundar, S. Ghosh, F. Mohajerani, L. N. Massenburg, T. Yang, P. S. Cremer, D. Velegol, and A. Sen, “Positive and negative chemotaxis of enzyme-coated liposome motors,” Nat. Nanotechnol. **14**, 1129–1134 (2019).

⁵¹X. Zhao, H. Palacci, V. Yadav, M. M. Spiering, M. K. Gilson, P. J. Butler, H. Hess, S. J. Benkovic, and A. Sen, “Substrate-driven chemotactic assembly in an enzyme cascade,” Nat. Chem. **10**, 311–317 (2018).

⁵²A. Solanki, T. Chen, and M. Riedel, “Computing mathematical functions with chemical reactions via stochastic logic,” PLOS ONE **18**, e0281574 (2023).

⁵³K. Rohlf, S. Fraser, and R. Kapral, “Reactive multiparticle collision dynamics,” Comput. Phys. Commun. **179**, 132 (2008).

Acknowledgements The authors thank Liyan Qiao for useful discussions. This work was supported in part by the National Natural Science Foundation of China (No.: 12274110), Natural Science Foundation of Zhejiang Province (No.: LHZSZ26A040002), and the Natural Sciences and Engineering Research Council of Canada.

Author contributions J. C. and R. K. contributed at all stages of this work. J. H. performed part of simulations.

Competing interests: The authors declare no competing financial interests.